Published online 25 January 2020 *Nucleic Acids Research, 2020, Vol. 48, No. 7* ***3789–3805***
doi: 10.1093/nar/gkaa035

circSamd4 represses myogenic transcriptional activity of PUR proteins

Poonam R. Pandey[1], Jen-Hao Yang[1], Dimitrios Tsitsipatis[1], Amaresh C. Panda[2], Ji Heon Noh[1,3], Kyoung Mi Kim[1,4], Rachel Munk[1], Thomas Nicholson[5], Douglas Hanniford[6], Diana Argibay[6], Xiaoling Yang[1], Jennifer L. Martindale[1], Ming-Wen Chang[1], Simon W. Jones[5], Eva Hernando[6], Payel Sen[1], Supriyo De[1], Kotb Abdelmohsen[1] and Myriam Gorospe[1,*]

[1]Laboratory of Genetics and Genomics, National Institute on Aging Intramural Research Program, National Institutes of Health, Baltimore, MD 21224, USA, [2]Institute of Life Sciences, Nalco Square, Bhubaneswar, Odisha, India, [3]Department of Biotechnology, Chonnam National University, Yeosu, Chonnam, Republic of Korea, [4]Department of Biological Sciences, Chungnam National University, Daejeon, Republic of Korea, [5]Institute of Inflammation and Ageing, MRC-ARUK Centre for Musculoskeletal Ageing Research, University of Birmingham, Birmingham, UK and [6]Department of Pathology, New York University School of Medicine, New York, NY, USA

Received August 22, 2019; Revised January 06, 2020; Editorial Decision January 09, 2020; Accepted January 13, 2020

ABSTRACT

By interacting with proteins and nucleic acids, the vast family of mammalian circRNAs is proposed to influence many biological processes. Here, RNA sequencing analysis of circRNAs differentially expressed during myogenesis revealed that *circSamd4* expression increased robustly in mouse C2C12 myoblasts differentiating into myotubes. Moreover, silencing *circSamd4*, which is conserved between human and mouse, delayed myogenesis and lowered the expression of myogenic markers in cultured myoblasts from both species. Affinity pulldown followed by mass spectrometry revealed that *circSamd4* associated with PURA and PURB, two repressors of myogenesis that inhibit transcription of the myosin heavy chain (MHC) protein family. Supporting the hypothesis that *circSamd4* might complex with PUR proteins and thereby prevent their interaction with DNA, silencing *circSamd4* enhanced the association of PUR proteins with the *Mhc* promoter, while overexpressing *circSamd4* interfered with the binding of PUR proteins to the *Mhc* promoter. These effects were abrogated when using a mutant *circSamd4* lacking the PUR binding site. Our results indicate that the association of PUR proteins with *circSamd4* enhances myogenesis by contributing to the derepression of MHC transcription.

INTRODUCTION

Even though >90% of the mammalian genome is transcribed, only ∼2% of transcripts encode protein (1). Recent progress in high-throughput RNA-sequencing and bioinformatic analysis has found that many of the noncoding transcripts form covalently closed circular (circ)RNAs. Tens of thousands of circRNAs have been identified in different cell types, and many display tissue-specific expression patterns and evolutionary conservation (2,3). CircRNAs have been shown to influence cellular processes such as proliferation, differentiation, senescence, as well as maintenance of cell pluripotency (4–6). Accordingly, several circRNAs have been implicated in physiology and disease (7–11). Despite this progress, the functions of circRNAs in most biological processes are unknown.

The skeletal muscle comprises nearly 40% of adult tissue, initially forming during embryonic development and continually regenerating throughout life via myogenesis (12). This process involves the specification of mesodermal precursor cells (satellite cells) into myoblasts, followed by subsequent differentiation and fusion of these cells into multinucleated myotubes. Early myogenesis is governed transcriptionally by the myogenic regulatory factors (MRFs) MYOD and MYF5, which mediate the initial specification of skeletal myoblasts, and by myogenin (MYOG), MRF4, and myocyte-specific enhancer factors (MEF2A and MEF2C), which induce differentiation of these specified cells (13). Later myogenic stages involve the fusion of the mononucleated myoblasts into multinucleated myotubes, the reorganization of cytoskeletal proteins, and the transcriptional expression of myosin heavy chain (MHC)

*To whom correspondence should be addressed. Tel: +1 410 558 8443; Email: gorospem@grc.nia.nih.gov

proteins, which function in muscle contraction. In addition to the myogenic transcription factors, myogenesis is tightly regulated at the post-transcriptional level through the actions of RNA-binding proteins (RBPs) and noncoding RNAs (ncRNA) such as miRNAs, lncRNAs, and circRNAs (14–16).

Numerous chronic age-associated muscular disorders, including sarcopenia, osteoarthritis, chronic heart failure, and chronic obstructive pulmonary disease (17–20), have been associated with aberrant myogenesis. We previously identified age-associated changes in circRNAs expressed in monkey skeletal muscle with advancing age and proposed that some of these circRNAs might influence muscle function during aging (21). Here, we employed RNA-sequencing analysis to identify circRNAs differentially expressed during muscle differentiation and conserved in human muscle cells. We found that depletion of the highly expressed *circSamd4* delayed myogenic progression and influenced late stages of muscle differentiation. Affinity pulldown followed by proteomic analysis identified *circSamd4*-interacting proteins including purine-rich binding proteins (PUR) alpha and beta (PURA, PURB), two proteins that bind to and repress myosin heavy chain (*Mhc*) promoter sequences. We propose that the progressive elevation in *circSamd4* during myogenesis contributes to sequestering PUR proteins, in turn facilitating a time-dependent derepression of the *Mhc* promoter and the increase in MHC production.

MATERIALS AND METHODS

Cell culture, differentiation, modulation of *circSamd4* levels

Proliferating C2C12 myoblasts were cultured in growth medium (GM), DMEM (Invitrogen) supplemented with 10% fetal bovine serum (Gibco), and antibiotics penicillin and streptomycin (Life Technologies). Proliferating, subconfluent C2C12 myoblasts were induced to differentiate by culture to high density and switch to differentiation medium [(DM), DMEM with 2% horse serum] for 3–6 days. Human myoblasts (22) were cultured in human skeletal muscle GM (Promocell) consisting of equal parts [DMEM with 10% FBS, 2 mM L-glutamine, 25 ng/ml FGFβ, 1 ng/ml EGF, and penicillin and streptomycin] and [Ham's F10 media containing 20% FBS] and antibiotics penicillin and streptomycin, and differentiated as described above with DM media. For silencing, 50 nM of control (Ctrl) or circSamd4 siRNAs (IDT) were transfected using Lipofectamine® 2000 (Thermo Fisher Scientific) into proliferating myoblasts 12 h before inducing differentiation. For overexpression, 1 μg of empty vector pcDNA3, pcDNA3-circSamD4 or deletion mutant pcDNA3-circSamD4Δ3 was transfected by electroporation (Amaxa Biosystems™) before inducing differentiation.

Identification of circRNA from RNA-seq analysis

The RNA from GM and DM cells was purified using the miRNeasy Mini kit (Qiagen) following the manufacturer's instructions. The RNA quality and quantity were assessed with the Agilent 2100-Bioanalyzer followed by removal of rRNA with the rRNA Depletion Nano kit (Qiagen). The cDNA library was prepared with the Ovation RNA-Seq System V2 (NuGEN) kit, and sequencing was performed on an Illumina HiSeq 2500 instrument (23); data are deposited in GSE92632 and GSE136004. Sequencing reads were mapped to the mouse genome (mm9) using TopHat2 (version 2.0.14) followed by identification of non-linear fusion junction reads using TopHat2. CircRNAs expressed in GM and DM samples were identified with the CIRCexplorer program (v1.10) as described previously (23).

RNA isolation and reverse transcription followed by quantitative PCR (RT-qPCR) analysis

RNA was isolated using TRIzol (Thermo Fisher Scientific) and subjected to reverse transcription (RT) and real-time quantitative (q)PCR analysis. After sequencing, divergent primers were designed to measure the relative expression levels of circRNAs and identify the junction sequence. Total RNA (2 μg) isolated from proliferating or differentiated cells was either left untreated or treated with RNase R (20 units, Epicentre) for 30 min at 37°C; RNA samples were then assayed by RT-qPCR analysis. Copy number was calculated by comparing Ct values of *circSamd4* with the concentration of transcripts of known abundance in cells, assuming 1500 copies of *Gapdh* mRNA per cell; these estimates were comparable to those described (24,25). Forward and reverse primers (Supplementary Table S1) were used to sequence PCR products and identify the junction sequence.

Expression of circRNAs in old and young human skeletal muscle

Quadriceps skeletal muscle was collected from lean elderly individuals (age 79 years ± 2; $n = 7$) intraoperatively during total knee arthroplasty surgery, and from lean young adults (age 25 years ± 4; $n = 7$) using a Bergström needle (UK Research Ethics Committee 14/ES/1044). The muscle tissue was snap-frozen in liquid nitrogen and ∼100 mg ground into a fine powder using a pestle and mortar under liquid nitrogen. Powdered tissue was immediately transferred to 1 ml of Trizol® reagent (Thermo Fisher Scientific) and homogenized using a Qiagen Tissue Ruptor. Total RNA was then extracted as described in the manufacturer's protocol (Trizol, Thermo Fisher Scientific) and resuspended in 30 μl of RNase-free water (Thermo Fisher Scientific). RNA concentration was quantified using a Nanodrop 2000 (Life Technologies).

For reverse transcription (RT), cDNA was synthesized from 60 ng of template RNA using a Tetro cDNA Synthesis Kit (Bioline) with random hexamers, as per the manufacturer's instructions. Relative RNA abundance was determined by two-step RT-qPCR analysis normalized to *GAPDH* mRNA levels; qPCR analysis was performed using a SensiFAST™ SYBR® No-ROX Kit (Bioline) following the manufacturer's protocol, using the primers listed in the Supplementary Figure S1; for *GAPDH* mRNA, the primers (sequence not disclosed) were from PrimerDesign Ltd. All reactions were performed using a Bio-Rad cycler (Bio-Rad) with a total reaction volume of 5 μl. Samples were assayed in triplicate and a non-template control was included for each gene of interest.

Plasmids

Briefly, plasmids to overexpress the *circSamd4* (pcDNA3-circSamd4) and deletion mutant *circSamd4Δ3* (pcDNA3-circSamd4Δ3) were constructed by cloning the *circSamd4* full and truncated sequences in the circRNA mini vector ZKSCAN1 (24) (Addgene #60649). Genomic DNA was isolated using DNeasy Blood & Tissue Kit (69504, Qiagen) and 25 ng of genomic DNA was used to amplify ∼519-bp genomic sequences upstream and downstream of *circSamd4* genomic coordinates using forward and reverse primers actgGGATCCTCGTGCTTGCGCCGGTTCCAA and actgaagcttGAATCATTAACCAATGGCAAC, respectively. The PCR products were cloned into the pcDNA3.0 circRNA mini vector ZKSCAN1. Constructs were verified by sequencing.

Antisense oligomer (ASO) pulldown and mass spectrometry analysis

For ASO pulldown, whole-cell lysates were incubated with 3 μg of a biotinylated control ASO (5′Biot-TTGGAACCGGCGCAAGCACGAGAATCATTAACCAATGGCA), or an ASO complementary to the *circSamd4* junction (Biot-TGGAACCGGCGCAAGCACGAGAATCATTAACCAATGGCAA) in 1× TENT buffer (10 mM Tris–HCl at pH 8.0, 1 mM EDTA at pH 8.0, 250 mM NaCl, 0.5% [v/v] Triton X-100) containing fresh protease and RNase inhibitors for 1 h at 25°C with rotation. The biotin-ASO complexes were then pulled down following addition of Streptavidin-coupled Dynabeads (50 μl, Invitrogen) and incubation for 30 min at 25°C with rotation. After extensively washing the Dynabeads, the samples were divided such that RNA and protein were isolated using TriPure (Sigma-Aldrich) and 2× SDS elution dye, respectively, added directly to the washed Dynabead-biotin-ASO complexes. The enrichment of RNAs in the circSamD4-ASO pulldown was assessed by RT-qPCR analysis and the circSamD4-ASO-associated proteins were subjected to mass spectrometry analysis. The presence of these enriched proteins was confirmed by Western blot analysis with and without digestion with RNase A, RNase R or both RNases.

Mass spectrometry raw data files were collected from analysis of each of four pulldown samples from human myoblasts and from each of four pulldown samples from mouse myoblasts. Proteins were searched against the Human UniProtKB protein sequence database (20 608 entries, 2016) and the mouse UniProtKB mouse protein sequences database (16 685 entries, 2016), respectively, obtained from NCBI website using the Proteome Discoverer 1.4 software (Thermo Scientific), using the SEQUEST and percolator algorithms. The searches were performed with the following parameters: Carbamidomethylation (+57.021 Da) of cysteines was fixed modification, and Oxidation and Deamidation Q/N-deamidated (+0.98402 Da) were set as dynamic modifications; the minimum peptide length was specified to be five amino acids; the precursor mass tolerance was set to 15 ppm, and fragment mass tolerance was set to 0.05 Da. The maximum false peptide discovery rate was specified as 0.01. The resulting Proteome Discoverer Report and assembled proteins with peptides sequences and matched spectrum counts are summarized in Supplementary Table S2.

Western blot analysis

Whole-cell lysates prepared in RIPA buffer were separated by SDS-PAGE and transferred onto nitrocellulose membranes (Invitrogen iBlot Stack). Incubations with primary antibodies recognizing MHC, MYOG, HSP90, LMNB2 (Lamin B) (Santa Cruz Biotech), MEF2C (Millipore), PURA, PURB, YB1, YBOX3 (Abcam) and HNRNPM (Invitrogen) were followed by incubations with the appropriate secondary antibodies conjugated with horseradish peroxidase (GE Healthcare). Signals were developed using Enhanced Chemiluminescence (ECL), and digitized images were captured using Kwik Quant Imager (Kindle Biosciences).

Immunofluorescence and single-molecule *in situ* hybridization microscopy

Cells were plated in 35-mm imaging dishes with glass bottoms (Idibi) in 100 μl PBS, fixed with 100 μl of 4% paraformaldehyde for 15 min at room temperature, washed twice with 100 μl of PBS, permeabilized and blocked with 0.2% Triton X-100 and 1% goat serum, incubated with 50 μl of anti-myosin antibody (1:500 Santa Cruz Biotech) and washed twice in PBS, incubated with 50 μl anti-mouse Cy3/AlexaFluor488 secondary antibody (Thermo Scientific), diluted 1:300 in PBS, and finally washed twice in PBS. Nuclei were stained using ProLong® Gold Antifade Mountant with DAPI (Thermo Scientific) and signals were visualized using a confocal microscope (ZEISS 710 LSM or 880 LSM) using a 65× objective for image acquisition.

For single-molecule *in situ* hybridization analysis, target probe sequences (BaseScope), preamplifier, amplifier, wash buffer, and target retrieval buffers are proprietary (Advanced Cell Diagnostics). Undifferentiated C2C12 myoblasts were harvested by standard methods, counted, and seeded in glass-bottom dishes (Cellvis, 55 mm, #0) at 300 000 cells per dish and cultured at 37°C/5% CO_2. Twenty-four hours after seeding, undifferentiated cells were fixed (undifferentiated controls) or media was changed to DMEM with 2% horse serum and Penicillin/Streptomycin for differentiation. Differentiation proceeded for 4 days before fixation. Samples were fixed in 10% neutral buffered formalin for 30 min at 25°C, washed three times with PBS, and dehydrated in 50%, then 70%, and then 100% ethanol. Fixed and dehydrated samples were stored in 100% ethanol at –20°C until staining. Samples were rehydrated in 70% ethanol, followed by 50% ethanol and finally in PBS. Samples were incubated with hydrogen peroxide for 10 min at 25°C; after rinsing twice in PBS, samples were hybridized and stained following the manufacturer's recommendations. Briefly, samples were treated with Protease III (ACD Bio) at 1:15 in PBS for 10 min at 25°C followed by rinsing in twice in PBS. Hybridization cassette (ACD Bio) and HybEZ oven (ACD Bio) were used for subsequent hybridization, preamplification and amplification. Single ZZ probes (ACD Bio, BaseScope) targeting linear *Samd4* mRNA (Ch1 – Green) or circular *circSamd4* (Ch2

- Red) were designed to target outside the circularized sequence or to the backsplice junction, respectively. *Samd4* mRNA or positive control [Ppib (Ch1) or Polr2a (Ch2)] probes were hybridized in the HybEZ oven set at 40°C for 2 h, followed by preamplification and amplification steps based on the ACD protocol. Chromogenic detection was performed using Duplex Green/Fast Red (ACD). Samples were then counterstained with hematoxylin 7211 (Richard Allen) for 10 s, rinsed briefly in water, then in 0.02% ammonia for 30 s, followed by another rinse with water. Coverslips were added with mounting medium (Vectamount) and cured for 24 h before imaging. Brightfield images were taken at 20× or 40× with a Nikon upright microscope equipped with a digital RGB camera.

Ribonucleoprotein immunoprecipitation (RIP) analysis

The association of *circSamd4* with endogenous PURA and PURB in cells was analyzed by ribonucleoprotein (RNP) immunoprecipitation (RIP) as described (27). Briefly, cells were lysed in polysome extraction buffer (PEB; 20 mM Tris–HCl at pH 7.5, 100 mM KCl, 5 mM $MgCl_2$ and 0.5% NP-40) supplemented with RNase and protease inhibitors. The cytoplasmic lysates were incubated with PURA (Abcam) and PURB (Abcam) or control IgG (Santa Cruz Biotech) antibodies at 4°C followed by incubation with protein-A-sepharose for 2 h at 4°C with rotation. After washes with ice-cold NT2 buffer [50 mM Tris–HCl (pH 7.5), 150 mM NaCl, 1 mM $MgCl_2$, 0.05% NP-40], the RNA in the RNP complexes was isolated using TriPure and used for RT-qPCR analysis as described above.

Biotin pulldown analysis

C2C12 whole-cell lysates (200 μg) were incubated with 250 ng of non-overlapping biotinylated RNA fragments (F1 to F8) custom-made from IDT to cover the entire sequence of *circSamd4* for 30 min at 25°C with rotation. Complexes were isolated with Streptavidin-coupled Dynabeads (Invitrogen) and the pulldown material was analyzed by western blot analysis using PURA and PURB antibodies.

Cell fractionation

Fractionation of nuclear and cytoplasmic components of C2C12 was performed according to the manufacturer's instructions (NE-PER kit, Thermo Fisher ScientificNE-PER kit, Thermo Fisher ScientificNE-PER kit, Thermo Fisher ScientificNE-PER kit, Thermo Fisher Scientific). The cytoplasmic and nuclear fractions were subjected to analysis of protein, RNA, and ribonucleoprotein complexes.

Luciferase assays

The dual *MHC* promoter reporter construct was obtained from GeneCopoeia and contains the *MHC* promoter driving expression of *Gaussia* luciferase with an SV40 promoter driving expression of *Renilla* luciferase. The reporter plasmid (pMH2-LUC-Renilla) (MPRM31645-PL01) (500 ng) along with 1 μg of either empty vector (pcDNA3), deletion mutant (pcDNA3-circSamd4Δ3) or wild-type (pcDNA3-circSamd4) plasmids, were transfected using Lipofectamine 2000® in 0.3×10^6 pre-seeded cells in a six-well plate; cells were harvested 48 h later in PLB lysis buffer (Promega) and RLuc and GLuc activities were measured by Dual Glo luciferase assay (Promega) following the manufacturer's protocol.

ChIP-qPCR analysis

ChIP assays were performed using a CHIP-IT High sensitivity kit (Active Motif, Inc.) as instructed by the manufacturer. Briefly, differentiated C2C12 cells were crosslinked with 1% formaldehyde for 10 min at 25°C, washed, and treated with glycine Stop-Fix solution. After resuspending in cell lysis buffer and incubating on ice for 10 min, pellets were sonicated to generate genomic DNA fragments. The chromatin was incubated for 16 h at 4°C with anti-PURA, anti-PURB (Abcam), or control IgG (Santa Cruz Biotechnology) antibodies. Protein G beads were then added to the antibody-chromatin complex and incubated for 3 h at 4°C. After extensive washes, the immunoprecipitated DNA complexes were eluted from the beads. DNA was purified by proteinase K digestion and the presence of *Mhc* II promoter (−270 to −450) regions as well as negative control *Syn2* region (TTS +200) (primers listed in Supplementary Table S1) were measured by qPCR analysis following the percentage input method as described (28,29).

Statistical analysis

All experiments were repeated at least 3 times unless otherwise stated. Quantitative data are represented as the mean ± SEM, and compared statistically by unpaired student's *t* test, using Prism GraphPad (7.0). Statistical significance is indicated in the figures as * ($P < 0.05$) and ** ($P < 0.005$). Dedicated statistics were applied to RNA-seq data analysis as specified in the legends.

RESULTS

The levels of conserved circRNA *circSamd4* increase in differentiated myoblasts

We used the mouse C2C12 myoblast model of myogenesis to investigate circRNAs implicated in skeletal muscle differentiation. C2C12 cells proliferate rapidly in normal growth media (GM), but upon reaching confluency and exposure to differentiation media (DM) in low serum, they stop dividing and progressively fuse, becoming multinucleated myotubes (myofibers) with a contractile phenotype (Figure 1A, top). To identify circRNAs differentially expressed during myogenesis, total RNA was isolated from C2C12 GM and DM (3 days) cultures and the circRNAs were identified by RNA-Seq as described (Materials and Methods) (Figure 1A, schematic; deposited in GSE92632 and GSE136004). The circRNAs were identified by the CIRCexplorer algorithm.

To monitor this myogenesis model, we studied the expression levels of myogenic markers MEF2C and MYOG, which regulate transcriptionally the myogenic protein expression program. The expression levels of these myogenic markers, as well as the myogenic protein myosin heavy

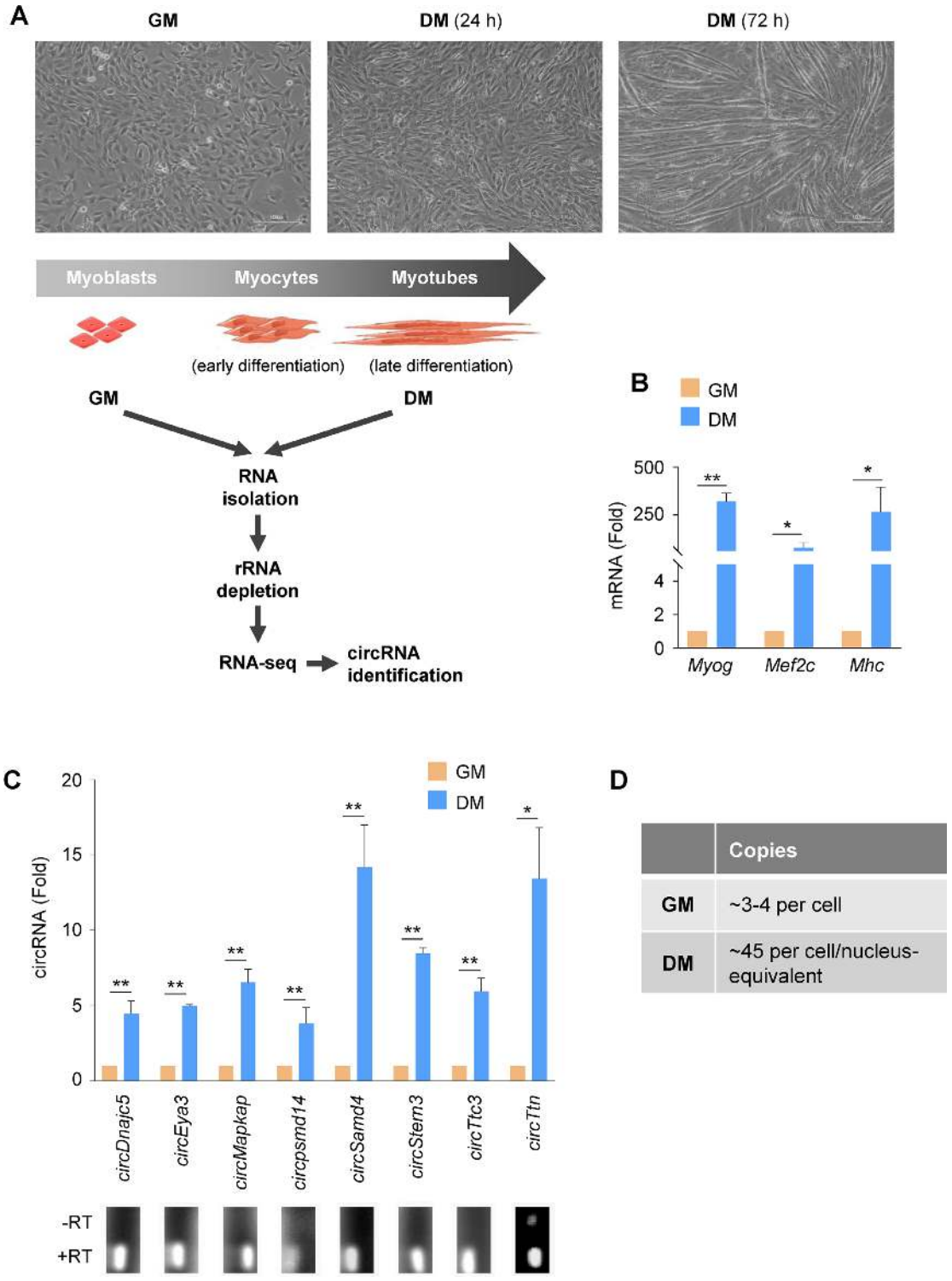

Figure 1. circRNAs expressed differentially during myogenesis. (**A**) Myoblast differentiation program; phase-contrast micrographs depicting cultures of C2C12 mouse myoblasts in proliferating conditions [growth medium (GM)], in early myogenesis after 24 h in differentiation medium (DM), and in late myogenesis, including myotubes, after 72 h in DM. *Schematic*, total RNA was prepared from proliferating C2C12 cells (GM) and from C2C12 cultures differentiating for 72 h (DM); after digestion of linear RNA, RNA pools enriched in circRNAs were sequenced (GSE92632 and GSE136004), and the circRNAs most highly expressed and most differentially abundant between GM and DM were validated by reverse transcription (RT) followed by real-time quantitative (q)PCR analysis. (**B**) Expression levels of myogenic markers *Myog*, *Mef2c*, *Mhc* mRNAs in C2C12 cultures, as assessed by RT-qPCR analysis. mRNA levels were normalized to the levels of housekeeping transcript *Gapdh* mRNA. (**C**) Expression levels of the indicated circRNAs, chosen among the most differentially abundant in DM relative to GM and most highly expressed overall. RT-qPCR analysis was performed by using divergent primers (Materials and Methods) in proliferating (GM) and differentiated (DM, 72 h) cultures. mRNA levels were normalized to the levels of housekeeping transcript *Gapdh* mRNA. Bottom, representative PCR products on 2% agarose gels; product specificity was assessed from reactions carried out in the presence or absence of reverse transcriptase (RT). (**D**) Quantification of copy numbers of *circSamd4* in C2C12 cultures in GM (per cell) and DM (per cell/nucleus-equivalent) by RT-qPCR analysis. Data in (B, C) are the means ± SEM from three independent experiments. $*P < 0.05$, $**P < 0.005$.

chain (MHC), were monitored by reverse transcription (RT) followed by real-time quantitative (qPCR) analysis. As shown, the corresponding mRNAs were drastically higher in C2C12 cultures by 3 days in DM relative to proliferating C2C12 (GM) cultures (Figure 1B, graph).

Among the circRNAs upregulated in differentiated C2C12 cells, we validated circRNAs that were abundant in this paradigm and those that were highly enriched in DM relative to GM. The levels of a subset of the validated circRNAs is shown (Figure 1C, including representative PCR products). We focused further efforts on *circSamd4* (*circID-mmu_circ_0000529*, *hsa_circ_0004846*), a circRNA derived from exon 3 of the mouse gene *Samd4* (NM_001037221.2; exon 2 in other transcript variants from the same mouse gene) that encodes the RBP SAMD4, for a number of reasons. There is 93% sequence similarity between human *circSAMD4* (*circSAMD4A*) and mouse *circSamd4* by BLAT analysis using circBase, indicating that it is conserved between both species (Supplementary Figure S1A). Moreover, in the human myoblast line KM155 (22), expression of *circSAMD4* increased similarly with myogenesis (DM relative to GM conditions; Supplementary Figure S1B) and followed similar kinetics (Supplementary Figure S1C). In addition, *circSAMD4* expression levels increased with age in human skeletal muscle, while *SAMD4* mRNA levels only changed moderately with age (Supplementary Figure S1D). Other connections to myogenesis include: (i) SAMD4 protein suppressed hallmarks of myotonic dystrophy (30); (ii) mutation in the mouse *Samd4* gene caused myopathy and uncoupled mitochondrial respiration (31); (iii) loss of SAMD4 in mice resulted in multiple developmental defects, including delayed bone development and decreased osteogenesis (32) and (iv) *circSAMD4* was recently implicated in the enhanced proliferation and stemness traits of osteosarcoma cells (33). The number of *circSamd4* copies in C2C12 myoblasts as well as the nucleus-equivalent copies in C2C12 myotubes was estimated as explained in Materials and Methods and revealed ∼3–4 copies of *circSamd4* per cell in GM populations, and ∼45 copies of *circSamd4* per cell/nucleus-equivalent in DM conditions (Figure 1D).

circSamd4

circSamd4 is generated by circularization of exon 3 of the *Samd4* gene located on chromosome 14 (mm9), *mmu_circ_0000529*. It is 519 nucleotides long and arises from head-to-tail splicing of exon 3 from NM_001037221.2, chr14 (hg19), region 47635951–47636470 (Figure 2A). In humans, *circSAMD4* arises from backsplicing of exon 3 of *SAMD4A* pre-mRNA (*hsa_circ_0004846*, NM_015589.6); it is also located on chromosome 14, 55168779–55169298 and is 519 nucleotides long. Of note, the same exon is exon 2 in other transcript variants from the same mouse and human genes. The *circSamd4* PCR product was sequenced to verify the presence of the backspliced junction (Figure 2A). Digestion using RNase R to degrade the linear RNA depleted almost all *Samd4* mRNA, but not *circSamd4* (Figure 2B), serving to confirm the circular nature of *circSamd4*. Despite the observed ∼14-fold increase in *circSamd4* levels (Figures 1C and 2C) during myogenesis, *Samd4* mRNA levels increased only 3-fold, suggesting that *circSamd4* expression was selectively upregulated during myogenesis (Figure 2C). The relative distribution of *circSamd4* in the nucleus and cytoplasm of C2C12 myoblasts and differentiated C2C12 myotubes was first assessed by RT-qPCR analysis, and included measurement of control transcripts *Actb* mRNA and lncRNA *7sk* to monitor the preparation of cytoplasmic and nuclear RNAs, respectively. As shown (Figure 2D), *circSamd4* levels increased markedly overall with differentiation, and it was found in both compartments, but was predominantly cytoplasmic.

This general pattern of distribution was verified by visualizing *circSamd4* as well as *Samd4* mRNA in proliferating and differentiated C2C12 cultures using the BaseScope single-molecule *in situ* hybridization (Materials and Methods). As shown in Figure 2E, *Samd4* mRNA signals were more abundant than *circSamd4* signals in proliferating myoblasts. By contrast, *circSamd4* signals increased overall during differentiation, and were found in both the nuclei and the cytoplasm of myotubes, but were more abundant in the cytoplasm.

circSamd4 promotes myogenesis

To investigate the biological function of *circSamd4* in myoblast differentiation, we designed several small interfering (si)RNAs targeting *circSamd4*, each spanning the backsplice junction (Figure 3A). Transfection of each of the three siRNAs reduced *circSamd4* levels significantly, but siRNA3 displayed the most potent reduction and did not suppress the levels of linear counterpart *Samd4* mRNA or the circRNA *circFn1* (Figure 3A and Supplementary Figure S2A). Given that *circSamd4*-directed siRNA1 and siRNA2 reduced *Samd4* mRNA levels moderately in C2C12 cells (Figure 3A, Supplementary Figure S2A–C), circSamd4 siRNA3 was chosen for subsequent studies.

After reducing *circSamd4* levels by transfection with *circSamd4* siRNA followed by exposure to DM conditions, microscopic analysis revealed that silencing *circSamd4* delayed myotube formation (Figure 3B). The activity levels of the myogenesis marker creatine kinase (CK) (Figure 3C), as well as the abundance of the myogenic markers *Myog*, *Mef2c* and *Mhc* mRNAs (Figure 3D) were also decreased when *circSamd4* was silenced. These results suggest that *circSamd4* contributes to the progression through myogenesis. In human KM155 myoblasts, knockdown of *circSAMD4* by siRNA3 similarly suppressed myogenesis, as determined by monitoring the levels of *SAMD4*, *MYOG,* and *MHC* mRNAs as well as CK activity (Supplementary Figure S2D–G), suggesting that *circSAMD4* also promoted human myogenesis. Immunofluorescence analysis provided additional evidence that myogenesis, as assessed by the myogenic marker MHC, was impaired in human myoblasts following *circSAMD4* silencing (Figure 3E). Western blot analysis further revealed that MHC and other myogenic markers (MYOG, MEF2C) were also reduced in human myoblasts in DM conditions after circSAMD4 siRNA transfections (Figure 3F). We then assessed whether ectopic overexpression of *circSamd4* in C2C12 influenced myogenesis by employing an expression vector designed to specifically express circRNAs (Materials and Methods). Although the magnitude of *circSamd4* overexpression achieved in

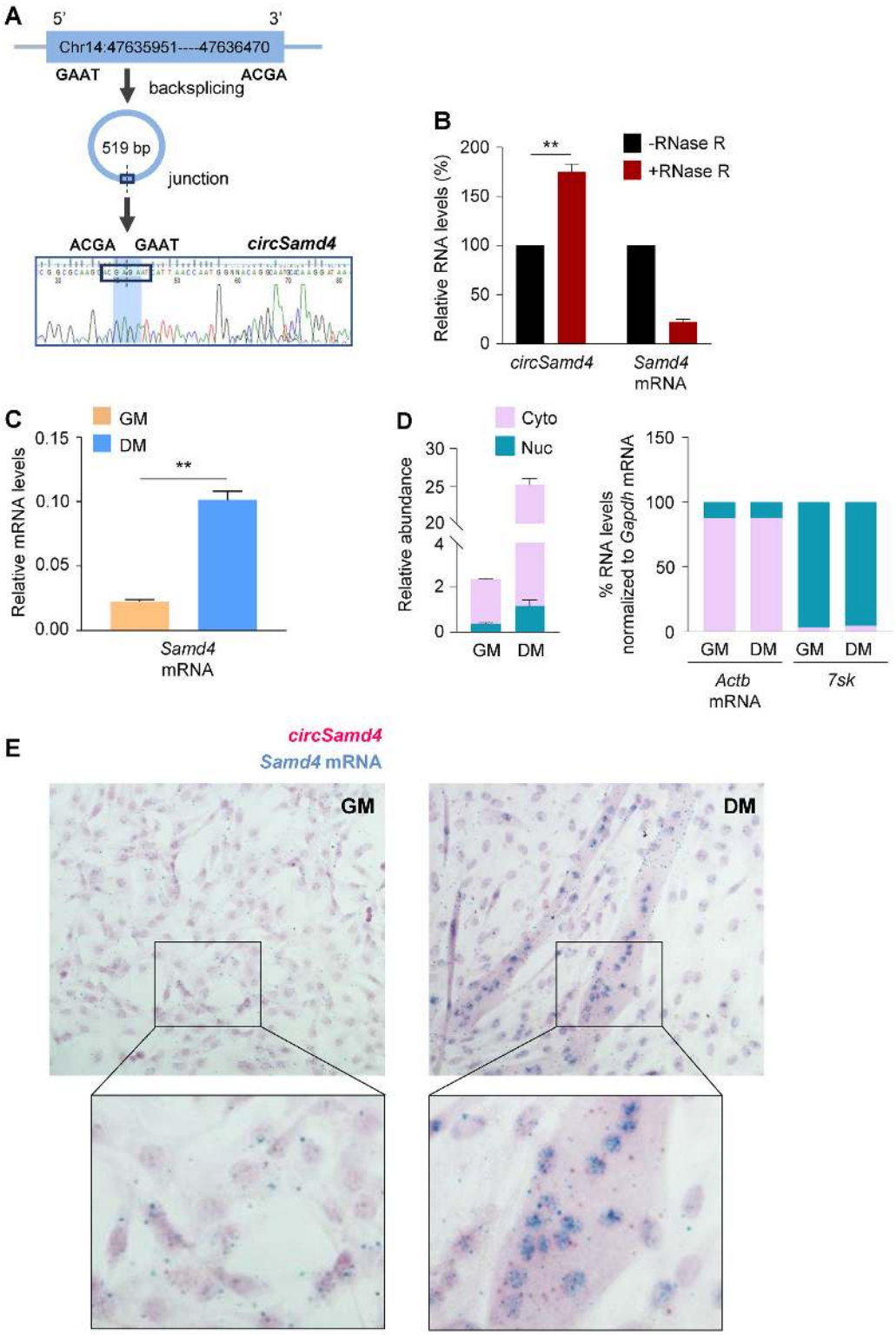

Figure 2. Characterization of *circSamd4*. (**A**) Schematic of exon 3 of *Samd4* mRNA, located on mouse chromosome 14 and giving rise to a 519-nucleotide long *circSamd4*, and detail of the sequence junction. (**B**) RT-qPCR results showing the abundance of *circSamd4* and *Samd4* mRNA in total RNA from C2C12 cells (GM) that were either left untreated or treated with RNase R. RNA levels were normalized to the levels of *Gapdh* mRNA. (**C**) Relative levels of *Samd4* mRNAs as measured by RT-qPCR analysis in GM and DM (72 h) C2C12 cultures. RNA levels were normalized to the levels of *Gapdh* mRNA in the same samples. (**D**) Relative levels of *circSamd4* in the nuclear (Nuc) and cytoplasmic/sarcoplasmic (Cyto) compartments of C2C12 GM and DM (72 h) cultures; the quality of the fractionation was assessed by monitoring the levels of a predominantly cytoplasmic transcript (*Actb* mRNA) and a predominantly nuclear lncRNA (*7sk*). (**E**) Brightfield micrographs to visualize *circSamd4* (red) and *Samd4* mRNA (blue) in proliferating (GM) and differentiated (DM) C2C12 cultures using the BaseScope single-molecule detection system (Advanced Cell Diagnostics, CA) (Materials and Methods). Nuclei are counterstained with hematoxylin. Data in (B, C) are the means ±SEM from three or more independent experiments. $^{**}P < 0.005$.

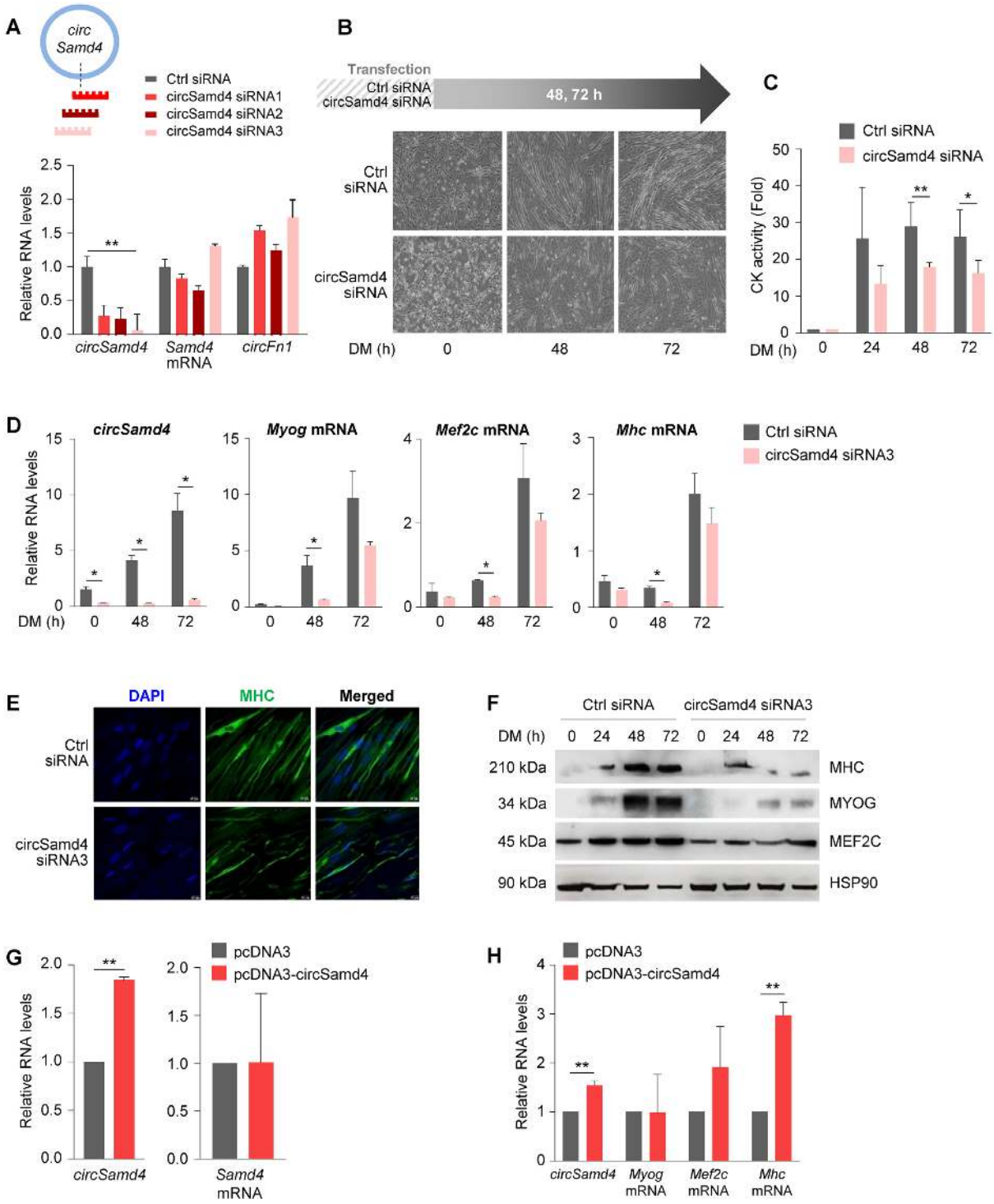

Figure 3. Silencing *circSamd4* reduces the levels of myogenic markers. (**A**) Schematic representation of 3 siRNAs designed to target the *circSamd4* junction. RT-qPCR analysis of the indicated circular and linear RNAs; C2C12 in GM were transfected with siRNAs, 8 h later the medium was switched to DM and 48 h after that, cells were collected for analysis. RNA levels were normalized to the levels of *Gapdh* mRNA. (**B–D**) Effect of silencing *circSamd4* on C2C12 differentiation. Ctrl and *circSamd4* siRNAs were transfected into C2C12 (GM) cells and differentiation was initiated 24 h later (time 0 h); 48 and 72 h into DM, phase-contrast micrographs were taken to monitor myotube formation (B), the levels of creatine kinase (CK) were measured at 0, 24, 48 and 72 h (C), and RNA was extracted to measure by RT-qPCR analysis the levels of *circSamd4* as well as myogenic markers *Myog*, *Mef2c*, and *Mhc* mRNAs, normalized to *Gapdh* mRNA levels (D). (**E**, **F**) The effect of silencing *circSAMD4* in human KM155 myoblasts (Supplementary Figure S1) on myogenesis was measured by immunofluorescence analysis of the myotube marker MHC in DM (72 h); nuclei were labeled with DAPI (E), and the levels of the myogenic proteins MHC, MYOG, and MEF2C were measured by western blot analysis (F). (**G**, **H**) Forty-eight hours after transfecting pcDNA3 (empty control) or pcDNA3-*circSamd4* into C2C12 cells, RT-qPCR analysis was used to assess the expression levels of *circSamd4* and *Samd4* mRNA (G) as well as those of myogenic markers *Myog, Mef2c*, and *Mhc* mRNAs, which were normalized to the levels of *Gapdh* mRNA (H). Data in (A, C, D, G, H) are the means ± SEM from three independent experiments. $^{*}P < 0.05$, $^{**}P < 0.005$.

C2C12 cells was modest (Figure 3G, left), it enhanced *Mhc* mRNA levels (Figure 3H), while it did not raise endogenous *Samd4* mRNA levels or ectopic linear exon 3 levels (Figure 3G, right; Supplementary Figure S3). Collectively, these data further support the notion that *circSamd4* contributes to myogenesis.

circSamd4 associates with PURA and PURB, transcriptional repressors of MHC production

To investigate how *circSamd4* modulates myogenesis, we sought to identify interacting partners, specifically *circSamd4*-associated proteins. We designed an antisense oligomer (ASO) complementary to the region spanning the *circSamd4* junction region in order to pull down the endogenous *circSamd4* from C2C12 myoblasts (Figure 4A, left) as well as *circSAMD4* from human KM155 myoblasts (Supplementary Figure S4). Following pulldown and confirmation by RT-qPCR analysis that *circSamd4* was selectively enriched in the pulldown material (Figure 4A, right), while *Samd4* mRNA was not enriched, we identified the associated proteins by mass spectrometry analysis (Figure 4B). Comparison of the ∼380 putative interacting proteins in mouse myoblasts and the ∼75 putative interacting proteins in human myoblasts (Supplementary Figures S4A, B and Supplementary Table S2) revealed a total of 53 proteins enriched in both the *circSamd4* (mouse myoblasts) and *circSAMD4* (human myoblasts) pulldowns preferentially in DM relative to GM (Figure 4B and Supplementary Table S2). Gene Ontology (GO) analysis revealed that some of the shared 53 proteins were capable of binding DNA and/or RNA (Figure 4C). Phenotype cluster analysis further showed that the proteins enriched in both groups play key roles in RNA processing (Supplementary Figure S4C).

Among the shared proteins, those displaying maximum peptide counts and playing potential roles in myogenesis or skeletal muscle metabolism included two candidates in the PUR family, PURA (Purα) and PURB (Purβ) (Figure 4D). These proteins were particularly interesting, as previous reports had suggested that PURA and PURB, which bind both RNA and DNA elements, were capable of binding the proximal promoters of the myosin heavy chain (*Mhc*) promoter in C2C12 cells and negatively regulated MHC production (34). Additionally, PUR proteins regulated MHC production transcriptionally in cardiac myocytes and were proposed to mediate a cardiac-restricted MHC production by preventing its expression in non-muscle cells (35).

We confirmed the interactions of PUR proteins with *circSamd4* using two different assays. First, we carried out pulldown analysis using ASOs, streptavidin-coated beads, and C2C12 lysates (GM and DM), followed by PURA and PURB western blot analysis. As shown in Figure 4E, *circSamd4*-directed ASO but not Ctrl ASO pulled down PURA and PURB, and this binding was increased in DM conditions. Other nucleic acid-binding proteins identified in the screen, including YBOX1 and YBOX3 were not enriched after testing of individual proteins in the *circSamd4* ASO pulldown samples (Supplementary Figure S4D), perhaps because YBOX proteins might interact with PUR proteins instead, as shown previously (36). Additionally, low levels of HNRNPM were recovered in both ASO fractions (Supplementary Figure S4D). We also confirmed that PUR RNP complexes contained *circSamd4* and not *Samd4* mRNA by digesting the samples with RNase A (which degrades all RNAs) and/or RNase R (which degrades linear RNAs preferentially). As shown in Figure 4F, PURA and PURB were no longer present if the complex was digested with RNase A, but they remained in the complex after digestion with RNase R, supporting the notion that they associated with the circular RNA.

Second, we studied these interactions by performing ribonucleoprotein (RNP) immunoprecipitation (RIP) analysis using antibodies that recognized PURA or PURB (Supplementary Figure S4E) and lysates from differentiated C2C12 cultures under IP conditions that preserved native complexes. We found a 12- to 14-fold enrichment in the levels of *circSamd4* RNA in PURA and PURB immunoprecipitated (IP) samples relative to the levels of *circSamd4* in the IgG IP samples (Figure 4G); importantly, *Samd4* mRNA was moderately enriched in PURB RIP samples (although not in PURA RIP samples) (Figure 4G). The abundant transcript *Gapdh* mRNA, encoding the housekeeping protein GAPDH, was not enriched in the IP materials, supporting the specificity of the association of *circSamd4* with PURA and PURB (Figure 4G). After fractionating nuclear and cytoplasmic compartments, RIP analysis revealed that PURA and PURB were capable of interacting with *circSamd4* in both the nucleus and the cytoplasm (Figure 4H). As shown in Supplementary Figure S4F, the levels of PURA and PURB increased with differentiation, and in DM they were detected in both compartments.

In control experiments, additional circRNAs that were initially identified as being upregulated during DM (Figure 1C) were not significantly enriched in PURA or PURB RIP samples (Supplementary Figure S5A), and YBOX3 RIP analysis did not show significant binding to *circSamd4* or *Samd4* mRNA (Supplementary Figure S5B). Finally, the levels of PURA and PURB, as well as the corresponding mRNAs, increased slightly with differentiation (Supplementary Figure S5C,D). Taken together, these data indicate that PURA and PURB preferentially associate with *circSamd4* during myogenesis.

A specific region in *circSamd4* promotes efficient binding of PUR proteins

In order to map the region(s) of interaction between *circSamd4* and PUR proteins, we prepared nonoverlapping biotinylated RNA fragments spanning the body of the circRNA (Materials and Methods). After incubation of each biotinylated RNA with whole-cell lysates prepared from differentiated C2C12 cultures, pulldown analysis using streptavidin beads followed by PURA and PURB western blot analysis revealed that both proteins associated most avidly with segment 3 (Figure 5A); we also observed weak binding of PURA to segments 6–8 (Figure 5A). The overall RNA-binding propensity and the prediction of potential RNA-binding regions of these PUR proteins were assessed using catRAPID analysis (37) (Supplementary Figure S6), yielding an overall interaction score of approximately 0.6 and supporting the observed RNA-binding properties of these proteins. Interestingly, the sequence of *circSamd4* seg-

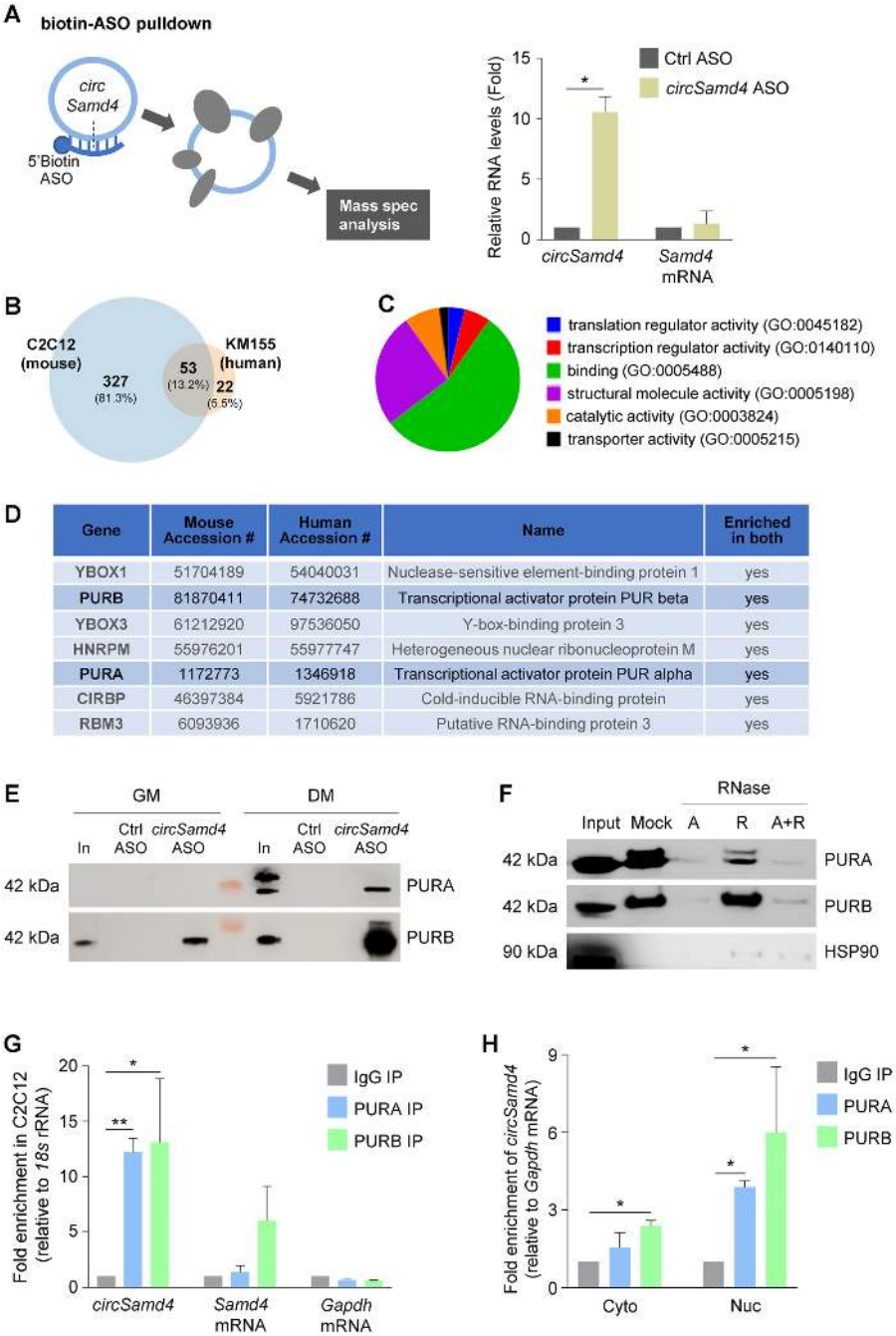

Gene	Mouse Accession #	Human Accession #	Name	Enriched in both
YBOX1	51704189	54040031	Nuclease-sensitive element-binding protein 1	yes
PURB	81870411	74732688	Transcriptional activator protein PUR beta	yes
YBOX3	61212920	97536050	Y-box-binding protein 3	yes
HNRPM	55976201	55977747	Heterogeneous nuclear ribonucleoprotein M	yes
PURA	1172773	1346918	Transcriptional activator protein PUR alpha	yes
CIRBP	46397384	5921786	Cold-inducible RNA-binding protein	yes
RBM3	6093936	1710620	Putative RNA-binding protein 3	yes

Figure 4. *circSamd4* interacts with transcription factors PURA and PURB. (**A**) *Left*, biotinylated antisense oligomers (ASOs) complementary to the junction of *circSamd4* and control (Ctrl) were incubated with C2C12 in GM as well as in DM. After affinity pulldown using streptavidin beads, *circSamd4*-interacting proteins were identified by mass spectroscopy. *Right*, levels of *circSamd4* enrichment in ASO pulldown samples, as assessed by RT-qPCR analysis of *circSamd4* (relative to the enrichment of *Gapdh* mRNA, a transcript that does not bind the ASOs and encodes a housekeeping protein) in the pulldown samples. Enrichment in *Samd4* mRNA was monitored in parallel. (**B**) Venn diagram representation of the proteins significantly enriched in the mass spec datasets identified after pulldown of *circSamd4* ASO vs Ctrl ASOs in mouse C2C12 myoblasts (left) and in human KM155 myoblasts (right) (Supplementary Figure S3; Materials and Methods). 53 proteins were shared in both mass spec datasets (intersection). (**C**) Pie chart represents GO functional categories of the 53 proteins at the intersection of both datasets. (**D**) Top 7 proteins shared in the mass spec datasets from mouse and human myoblast pulldowns (Supplementary Table S2 and Supplementary Figure S3A and S3B). (**E**) Western blot analysis of the interaction of *circSamd4* with PURA and PURB present in DM and GM lysates, as assessed after biotin-ASO pulldown followed by western blot analysis of PURA and PURB levels in the pulldown material. Input (*In*), 5 μg of GM or DM lysates (C2C12). (**F**) The interaction of PURA and PURB with *circSamd4* was assessed as explained in panel (E), except that lysates were treated with RNase A and/or RNase R before pulldown followed by western blot analysis. (**G**) For RIP (ribonucleoprotein immunoprecipitation) analysis, IP was performed using DM C2C12 lysates and either IgG (control) antibodies or antibodies recognizing PURA or PURB; the presence of *circSamd4* and *Samd4* mRNA (as well as control *Gapdh* mRNA) in the IP material was measured by RT-qPCR analysis. Enrichments were normalized to the levels of *18s* rRNA. (**H**) After fractionating nuclei and cytoplasm, RIP analysis was carried out as explained in (G) to measure the interaction of PURA and PURB with *circSamd4* in the nucleus and the cytoplasm. Data in (A,G,H) are the means ±SEM from three independent experiments. $*P < 0.05$, $**P < 0.005$.

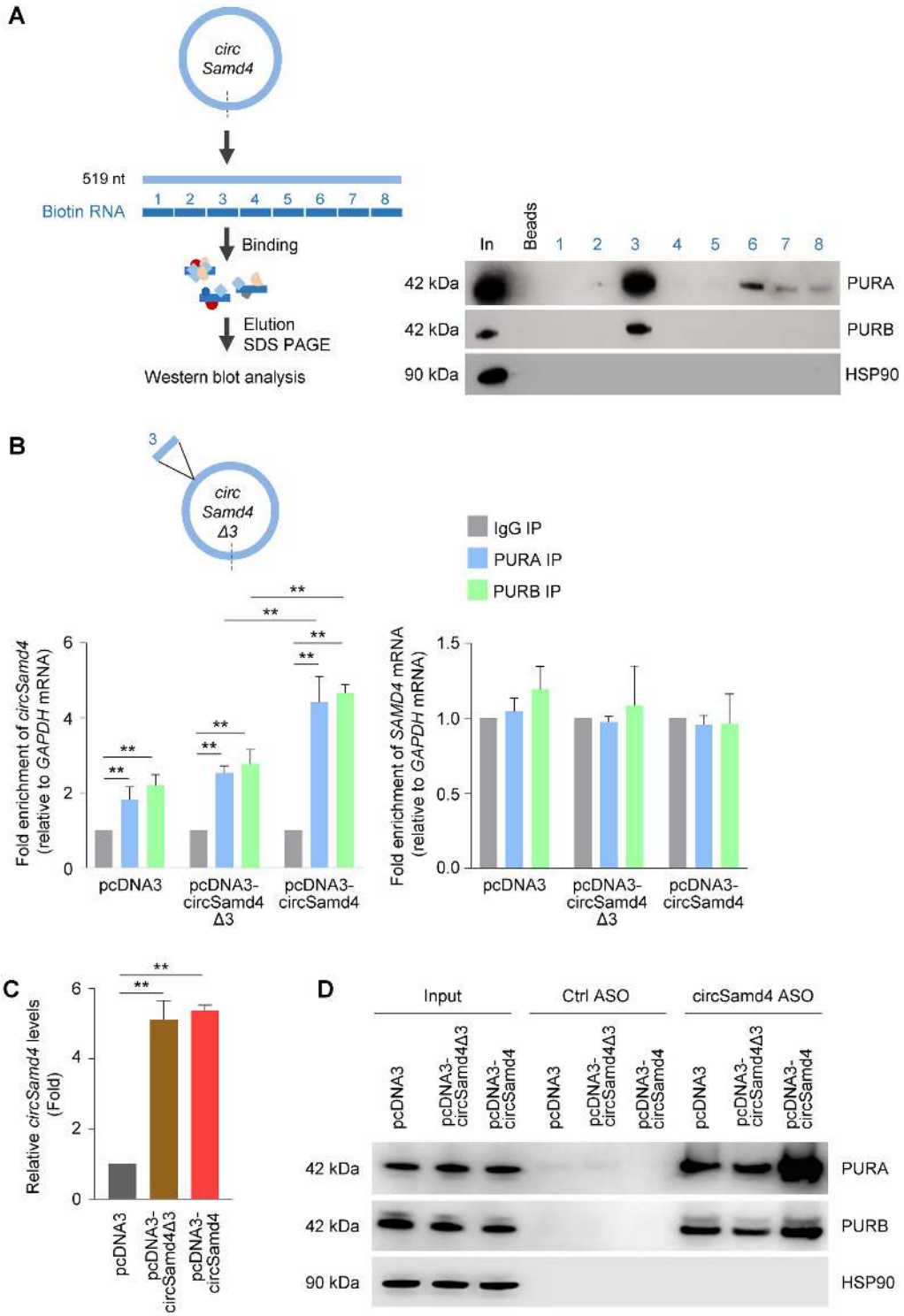

Figure 5. PUR proteins predominantly associate with a specific region of *circSamd4*. (**A**) Schematic of biotin pulldown of PURA and PURB using nonoverlapping biotinylated RNAs (each ∼65 nt long) tiling the length of *circSamd4*. Following incubation of the biotinylated RNAs with C2C12 DM lysates, bound proteins were pulled down using streptavidin beads and the presence of PURA and PURB was assessed by western blot analysis. Input (*In*) was 2 μg of DM lysates; Beads only (*Beads*), no biotinylated RNA. (**B**, **C**) Schematic, *circSamd4Δ3* bearing a deletion of segment 3. By 24 h after transfecting HeLa cells with vectors (2 μg) to overexpress *circSamd4* and *circSamd4(Δ3)*, RIP analysis was used to measure *circSamd4* (left graph) and *SAMD4* mRNA (right graph) bound to PURA and PURB relative to the levels of *GAPDH* mRNA (B). The levels of *circSamd4Δ3* and *circSamd4* expressed in HeLa cells 24 h after transfection of plasmids pcDNA3-circSamd4Δ3 and pcDNA3-circSamd4, respectively, were measured by RT-qPCR analysis and normalized to *GAPDH* mRNA levels (C). (**D**) Following overexpression of *circSamd4* and *circSamd4Δ3* as explained in panel (B), biotin-ASO pulldown was carried out to confirm the interaction of PURA and PURB with *circSamd4* in C2C12 lysates as shown by Western blot analysis. The levels of the housekeeping protein HSP90 were assessed as a background control protein. Input was 2 μg of DM lysates. Data in (B,C) are the means ±SEM from three independent experiments. $^{**}P < 0.005$.

ment 3 contains some of the trinucleotides (GGA, AAG, CGG, CAG) identified by SELEX (38) as being preferentially bound by PURA, although they were not found as triplet repeats within *circSamd4*.

Further evidence that endogenous PUR proteins bound segment 3 was obtained by employing constructs that overexpressed full-length *circSamd4* (pcDNA3-circSamd4) or a truncated circRNA lacking fragment 3, *circSamd4Δ3* (expressed from pcDNA-circSamd4Δ3). To test if fragment 3 was the region of interaction, we did not use C2C12 cells, as modulating *circSamd4* alone had confounding effects on myogenesis. Instead, we transfected the constructs into human cervical carcinoma HeLa cells and 24 h later performed RIP analysis using anti-PURA and anti-PURB antibodies; as shown (Figure 5B, left), only the full-length *circSamd4* was enriched in the PURA and PURB IP samples, as binding to the truncated RNA *circSamd4Δ3* was equivalent to the binding observed with the empty vector. The interaction of PUR proteins with linear *Samd4* mRNA was unchanged regardless of whether the full-length or the truncated circRNA was overexpressed (Figure 5B, right) further supporting the notion that PURA and PURB associated with segment 3 of *circSamd4*. Both *circSamd4Δ3* and *circSamd4* were expressed at approximately the same levels (Figure 5C). Additional analysis of the consequences of PURA and PURB interacting with *circSamd4* was pursued by overexpressing these plasmids, as well as empty vector pcDNA3 (Figure 5C) in HeLa cells followed by ASO pulldown. In keeping with earlier data, both PURA and PURB were more enriched in pulldowns from cultures expressing full-length *circSamd4* than in cultures expressing *circSamd4Δ3,* indicating that this segment was important for protein binding (Figure 5D). Together, these data suggest that region 3 in *circSamd4* is important for efficient binding of PURA and PURB.

PURA and PURB repress the transcription of *Mhc* mRNA, *circSamd4* alleviates this repression

While PUR proteins can promote transcription of target genes, they can also suppress transcription, as shown for *Mhc* (34). Accordingly, silencing PURA or PURB in C2C12 myoblasts led to increased expression of both *Mhc* RNA (Figure 6A) and MHC protein (Figure 6B), supporting earlier reports that PURA and PURB suppress transcription of the *Mhc* gene (34); under these conditions, *circSamd4* and *Samd4* mRNA levels remained unaltered. Further evidence of this regulatory paradigm came from analysis of a heterologous luciferase reporter in which the *Mhc* promoter drove Gaussia luciferase (GLuc) activity; Renilla luciferase (RLuc) expressed from the same vector, served as the transfection control. As shown in Figure 6C, silencing of either PURA or PURB significantly elevated *Mhc*-driven expression of luciferase 1.8- and 1.3-fold, respectively, supporting the notion that PURA and PURB repress MHC expression. Importantly, the converse did not occur, as *circSamd4* silencing in C2C12 cells did not influence the production of *Pura* or *Purb* mRNAs (Figure 6D) or PURA or PURB proteins (Figure 6E). Likewise, overexpression of *circSamd4* in C2C12 cells did not influence the levels of PURA or PURB (Figure 6F). These data indicate that PURA and PURB repress *Mhc* transcription and hence MHC expression levels.

We then hypothesized that binding of *circSamd4* might impact upon PURA and PURB function. To test this possibility, we used the luciferase reporter construct in the presence of either full-length *circSamd4* or *circSamd4Δ3*. As shown, only expression of full-length *circSamd4* was able to promote reporter gene expression in differentiated C2C12 cultures, while expression of the deletion mutant *circSamd4Δ3* or the empty vector control failed to do so (Figure 7A). Furthermore, expression of *circSamd4* increased MHC expression in C2C12 cells, while expression of *circSamd4Δ3* did not (Figure 7B). These data suggest that *circSamd4* might be sequestering PURA and PURB proteins, thereby enabling MHC production during myogenesis, while deletion mutant *circSamd4Δ3*, by being unable to bind PURA and PURB, failed to derepress MHC production.

To test these possibilities directly, we assessed if *circSamd4* influenced the binding of PUR proteins to the *Mhc* promoter. Chromatin immunoprecipitation (ChIP) was performed followed by qPCR analysis (Materials and Methods) of the conserved *Mhc* proximal promoter region containing the dNRE-S elements, a major binding site of PURA and PURB in C2C12 myoblasts (34). This analysis revealed that binding of PURA and PURB to the *Mhc* promoter increased significantly upon depletion of *circSamd4* in C2C12 cells under DM conditions (Figures 7C and D), supporting the view that *circSamd4* can relieve the transcriptional inhibition of *Mhc* transcription by PURA and PURB. Conversely, overexpression of *circSamd4* in C2C12 cells had the opposite effect, as ChIP analysis revealed that PURA and PURB binding to the *Mhc* promoter decreased after *circSamd4* overexpression (Figures 7E and F). Collectively, these data support a model whereby in proliferating myoblasts (GM) PURA and PURB suppress the *Mhc* promoter and MHC production. During myogenesis, *circSamd4* levels rise and *circSamd4* associates with a fraction of nuclear and/or cytoplasmic PURA and PURB, two transcriptional repressors of the myogenic protein MHC, which is required for myotube formation. By contributing to the derepression of MHC production, *circSamd4* helps to establish later stages of myogenesis (Figure 7G).

DISCUSSION

CircRNAs are increasingly recognized as being implicated in gene regulatory networks influencing development and disease. Here, we investigated circRNAs associated with skeletal myogenesis, a process whereby myoblasts differentiate into myotubes. We found that *circSamd4* increased robustly during skeletal muscle differentiation and associated with PURA and PURB, two proteins that bind and transcriptionally repress the *Mhc* promoter and thereby suppress myogenic differentiation. We propose a model (Figure 7G) in which *circSamd4*, accumulating during myogenesis, associates with PURA and PURB, thereby contributing at least in part to the derepression of *Mhc* transcription, the rise in MHC levels, and the promotion of myogenesis. To support this model, we present evidence that silencing *circSamd4* delayed myogenesis, reduced the expression of myo-

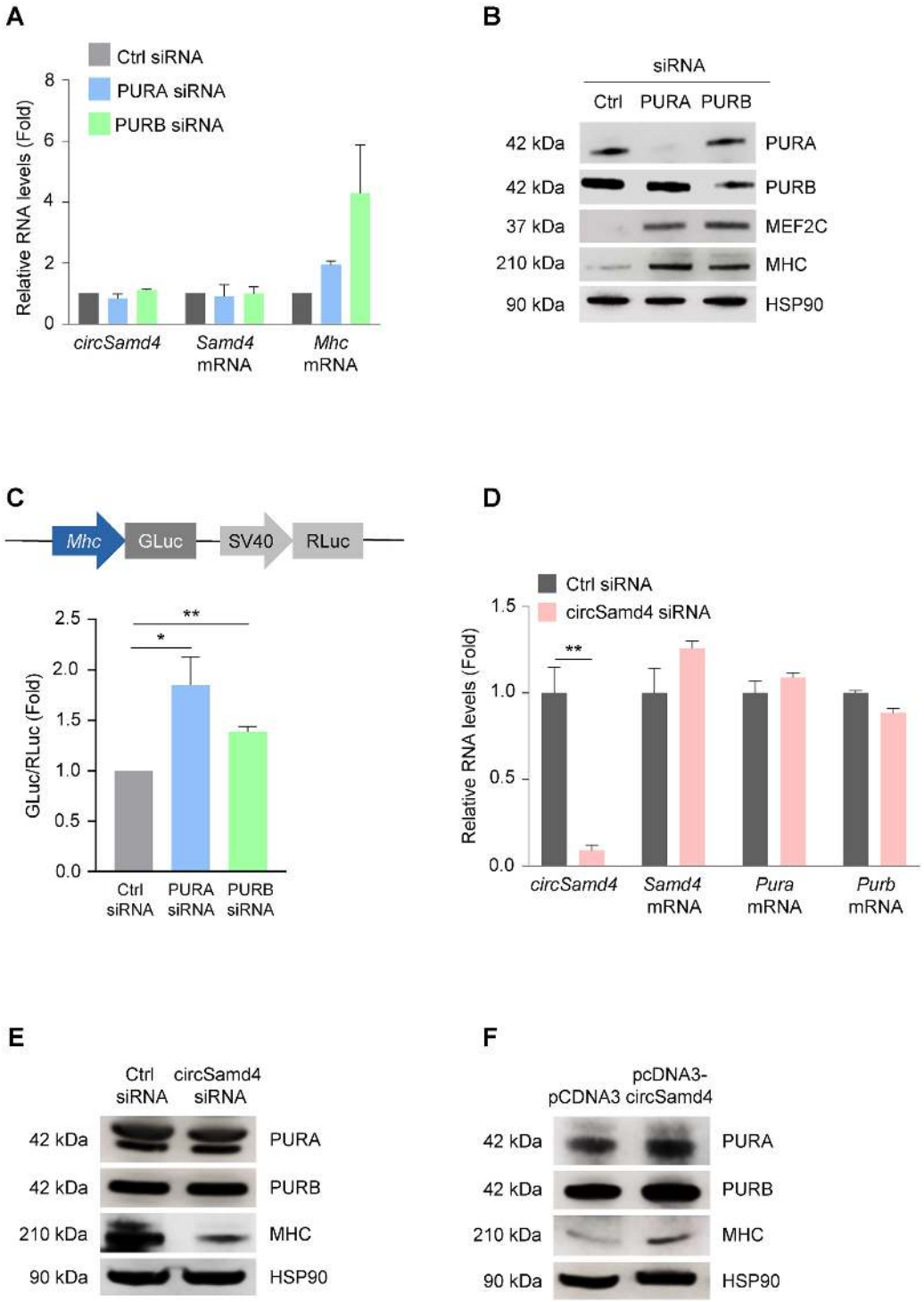

Figure 6. PUR proteins suppress MHC production transcriptionally. (**A**, **B**) C2C12 myoblasts were transfected with siRNAs to silence PURA and PURB; 48 h later, the levels of *circSamd4*, *Samd4* mRNA, and *Mhc* mRNA were assessed by RT-qPCR analysis and normalized to *Gapdh* mRNA (A). Western blot analysis was used to evaluate the levels of PURA, PURB, MEF2C, MHC, and loading control HSP90 (B). (**C**) Schematic of the *Mhc* promoter reporter construct (pmh2-GLuc-RLuc) (GeneCopoeia Inc.) used to evaluate *MHC* transcription. GM C2C12 cells were transfected with 1 μg of plasmid pmh2-GLuc-RLuc in cells expressing normal levels or silenced PURA and PURB as explained in panel (A); 8 hours later, cells were switched to DM media, and 24 h after that, promoter activity was measured. GLuc levels were normalized to RLuc levels in each group; data were then plotted as the difference in GLuc/RLuc ratios in the Ctrl siRNA transfection group compared with PURA or PURB silencing groups. (**D**) C2C12 cells were transfected with control (Ctrl) siRNA or *circSamd4* siRNA; 48 h later, the expression levels of *Pura* and *Purb* mRNAs, normalized to the levels of *Gapdh* RNA, were measured by RT-qPCR analysis and plotted. (**E**, **F**) Effect of silencing *circSamd4* on the expression of PURA, PURB, and MHC; 48 h after transfecting GM C2C12 cells with control (Ctrl) siRNA or *circSamd4* siRNA, the levels of *circSamd4*, and *Samd4*, *Pura*, and *Purb* mRNAs were assessed by RT-qPCR analysis (E) and the levels of proteins PURA, PURB, MHC, and loading control HSP90 by western blot analysis (F). Data in (A,C,D) are the means ±SEM from three or more independent experiments. $^{*}P < 0.05$, $^{**}P < 0.005$.

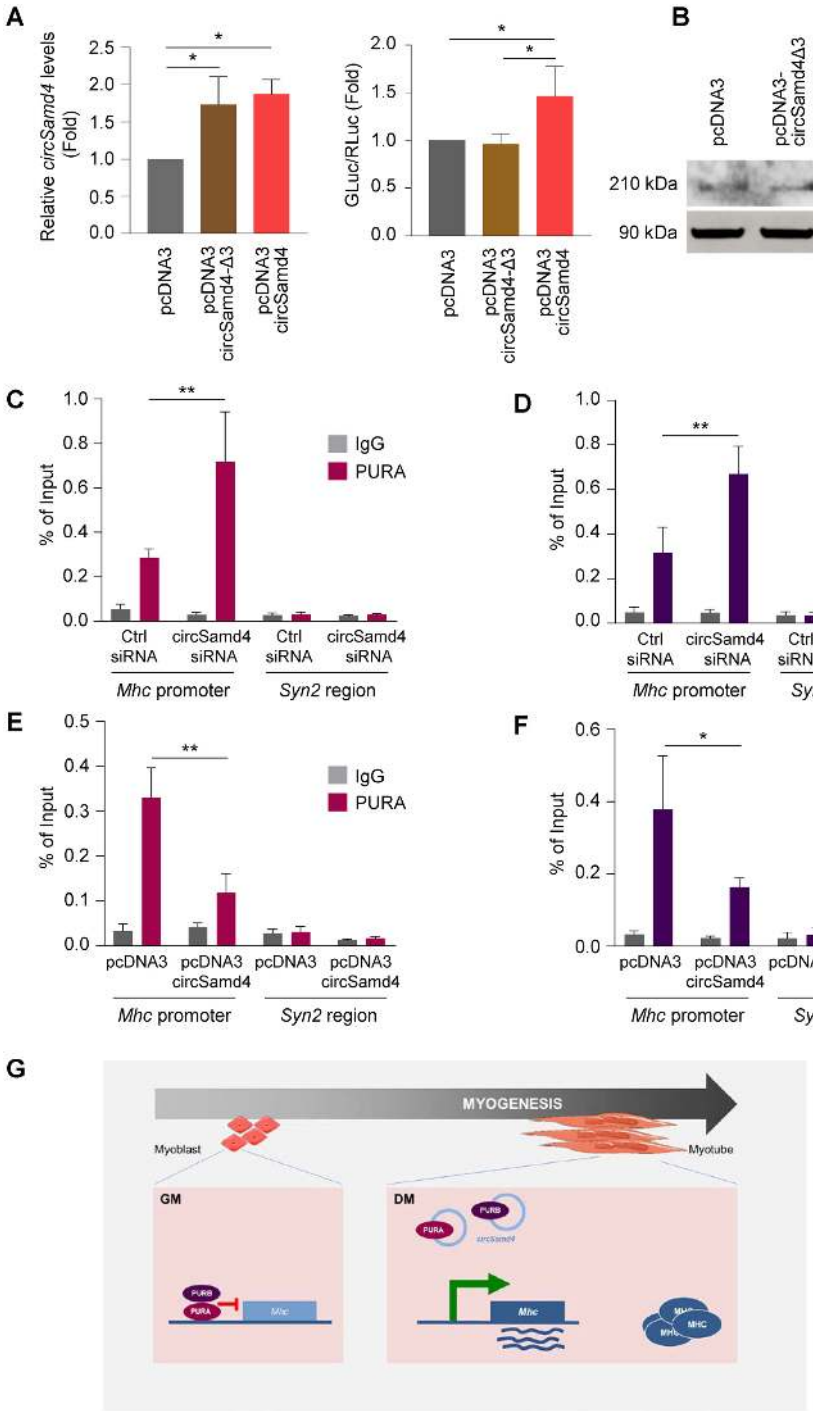

Figure 7. *circSamd4* binds PUR proteins, derepressing *Mhc* gene transcription. (**A**) Activity of the *Mhc* promoter, as determined by monitoring luciferase activity after transfecting 500 ng of reporter pMH2-LUC-Renilla (Figure 6C) into C2C12 cells that had been transfected 24 h earlier with parent vector pcDNA3 or with vectors expressing *circSamd4* or *circSamd4-Δ3* (left graph). Eight h after transfection of the reporter construct, the cells were switched to DM media for 24 h and promoter activity was measured; as above (Figure 6C), GLuc was normalized to RLuc and these ratios were plotted relative to the ratios measured in the empty vector group (right graph). (**B**) The levels of MHC in the different transfection groups shown in panel (A) were assessed by western blot analysis and HSP90 levels were shown as the loading control. (**C–F**) ChIP-qPCR analysis of the association of PURA and PURB with the *Mhc* proximal promoter region (−270/−450). Following crosslinking (Materials and Methods), antibodies recognizing PURA (C, E) or PURB (D, F) or control nonspecific rabbit IgG antibodies were used to immunoprecipitate sheared chromatin from C2C12 myoblasts in which *circSamd4* was silenced (C, D) or overexpressed (E, F). Specific oligonucleotide primers were used to amplify the region of interaction with PURA and PURB. ChIP-qPCR data were calculated using percentage of input; the TTS region of the neuron-specific gene *Syn2* (region +200 TTS), which encodes the protein SYN2 (Synapsin), was assayed as a non-target negative control. (**G**) Summary model. In myoblasts (GM), virtually undetectable levels of *circSamd4* permit the repression of the *Mhc* promoter by PURA and PURB. As myogenesis progresses (DM), the rise in *circSamd4* leads to binding of a fraction of PURA and PURB away from the *Mhc* promoter, thereby helping to derepress *Mhc* transcription and enabling the accumulation of *Mhc* mRNA and the production of MHC, a key protein in mature myotubes. Data in (A, C–F) are the means ±SEM from three or more independent experiments. $*P < 0.05$, $**P < 0.005$.

genic factors (e.g. *Myog*, *Mef2c* and *Mhc* mRNAs, as well as the encoded proteins) (Figure 3) and helped to preserve the binding of PURA and PURB to the *Mhc* promoter (Figure 7C and D), keeping MHC levels low; conversely, overexpression of *circSamd4* lowered PURA and PURB binding to the *Mhc* promoter and increased MHC production (Figure 7B, E and F). A mutant *circSamd4* lacking the site of interaction with PURA/B (*circSamd4Δ3*) was unable to rescue the effects of *circSamd4* on myogenesis.

The mechanism whereby *circSamd4* promotes myogenesis remains to be studied in molecular detail. For example, how specifically the production of *circSamd4* from *Samd4* pre-mRNA rises during differentiation while *Samd4* mRNA levels rise comparatively less (Figure 2). The possible involvement of myogenic splicing factors in the production of *circSamd4* is not known at present. Whether some of the additional *circSamd4*-binding proteins that have splicing activity, such as HNRNPM (Figure 4D), TRA2B, SRSF6 or others (Supplementary Figure S4A, B; Supplementary Table S2) are implicated in the generation of *circSamd4* also warrants future investigation.

The lower abundance of *circSamd4* in the nucleus (estimated at ∼2 molecules) suggests that nuclear *circSamd4* cannot alone suppress the binding of all of the nuclear PURA and PURB to the *Mhc* promoter. Instead, *circSamd4* likely cooperates with other factors to prevent the transcriptional repression of *Mhc* by PURA and PURB, even though these cooperating factors were not identified in this study. Alternatively, given that cytoplasmic *circSamd4* is more abundant (∼20-fold than the nuclear *circSamd4*; Figure 2D and E), it is possible that *circSamd4* binds to and sequesters PURA/B in the cytoplasm, and thus it prevents PURA/B from repressing *Mhc* transcription in the nucleus, or perhaps *circSamd4* helps export PUR proteins to the cytoplasm. Supporting these possibilities, PURA and PURB were also found to reside in both compartments (supplementary Figure S4F) and *circSamd4* was found to interact with PUR proteins in both the nucleus and the cytosol (Figure 4H). Additional related questions that warrant study in biochemical detail include how the affinity of PURA and PURB for *circSamd4* compares to its affinity for the *Mhc* promoter during myogenesis. In a recent study, *circSAMD4* was found to promote osteosarcoma by associating with microRNA miR-1244 (33). Whether PURA and PURB binding influences the binding of myogenic microRNAs to *circSAMD4* or *circSamd4* also deserves future study.

PURA and PURB are highly conserved proteins, from bacteria to mammals, and are found in virtually every tissue (www.genecards.org), although PURA appears to be more abundant. The PUR protein family also includes PURG, although PURG was not found to bind *circSamd4* in our screen, and it seems less abundant in tissues overall. PURA and PURB interact with both single-stranded DNA and RNA and influence molecular processes such as DNA replication, gene transcription, cytoplasmic RNA transport, and compartmentalized mRNA translation (39,40). Besides mRNAs, PURA was found to interact with lncRNA *BC1* in rodents and the cognate lncRNA *BC200* in humans (41,42), as well as with other proteins (43). It will be interesting to study whether *circSamd4* mobilizes PURA and PURB to the cytoplasm of myoblasts and enables cytoplasmic functions for PURA and PURB in mRNA transport or translation, particularly during later stages of myogenesis when MHC is strongly expressed.

Previous work indicated that PUR proteins repressed the transcription of *α-MHC* mRNA and the translation of α-MHC in cardiac myocytes and may thus prevent its expression in non-muscle cells (35). In this regard, it will also be important to establish the possible impact of PURA and PURB, and by extension of *circSamd4*, on the production of the different sarcomeric MHC gene variants (34) and to find out if other promoters inhibited by PUR proteins are also derepressed by an increase in *circSamd4* levels. In addition, endogenous PURA and PURB were necessary to fully repress full-length smooth muscle *ACTA* (α-Actin) promoter in cultured fibroblasts but to a lesser extent in vascular smooth muscle cells (44). Indeed, the effects of PUR-*circSamd4*-mediated gene regulation may be broadly relevant to other tissue types such as cardiomyocytes, fibroblasts, neurons, myeloid cells, and vascular smooth muscle cells in which PUR proteins are expressed and are functional (35,40,44,45).

Future studies analyzing comprehensively *circSamd4*-interacting proteins and RNAs may uncover its role in skeletal muscle formation and in muscle disorders such as myotonic dystrophy (DM) and facioscapulohumeral muscular dystrophy (FSHD). As several chronic skeletal muscle dysfunctions are associated with changes in MHC production, interventions to modulate *circSamd4* function may be therapeutically valuable in disease conditions. Finally, work is underway to understand the mechanisms driving the age-dependent decline in MHC levels, given that *circSAMD4* abundance increases with age (Supplementary Figure S1D). A comprehensive understanding of *circSamd4* biogenesis, interaction partners, and impact on myogenic gene expression programs will guide novel circRNA-centered interventions in age- and disease-associated loss of muscle function.

DATA AVAILABILITY

RNA-seq data has been deposited in GEO (https://www.ncbi.nlm.nih.gov/geo/) with accession numbers GSE92632 and GSE136004.

SUPPLEMENTARY DATA

Supplementary Data are available at NAR Online.

ACKNOWLEDGEMENTS

The authors appreciate the assistance provided by Dr Anup Mahurkar from the University of Maryland and Dr Dhiraj Kumar from MD Anderson Cancer Institute.
Author contributions: P.R.P. and A.C.P. conceived the study; P.R.P., K.A. and M.G. designed experiments and analyzed data; P.R.P., J.H.Y. A.C.P., R.M., D.T., T.N., D.H., D.A. and X.Y performed experiments; A.C.P., J.H.Y., J.H.N., K.M.K., J.L.M. and M.W.C. provided technical support; S.D. performed informatics analysis; P.S., K.A., S.W.J. and E.H., contributed intellectually; and P.R.P. and M.G. wrote the manuscript.

FUNDING

NIA-IRP, NIH; S.W.J. received funding from Versus Arthritis [21530, 21812]; D.H., D.A. and E.H. were supported by NIH/NCI [P30CA016087, S10 OD021747NIH, R01CA2022027]; Leveraged Finance Fights Melanoma-MRA Team Science Award. The open access publication charge for this paper has been waived by Oxford University Press – *NAR* Editorial Board members are entitled to one free paper per year in recognition of their work on behalf of the journal.

Conflict of interest statement. None declared.

REFERENCES

1. Atianand,M.K. and Fitzgerald,K.A. (2014) Long non-coding RNAs and control of gene expression in the immune system. *Trends Mol. Med.*, **20**, 623–631.
2. Memczak,S., Jens,M., Elefsinioti,A., Torti,F., Krueger,J., Rybak,A., Maier,L., Mackowiak,S.D., Gregersen,L.H., Munschauer,M. *et al.* (2013) Circular RNAs are a large class of animal RNAs with regulatory potency. *Nature*, **495**, 333–338.
3. Salzman,J., Chen,R.E., Olsen,M.N., Wang,P.L. and Brown,P.O. (2013) Cell-type specific features of circular RNA expression. *PLoS Genet.*, **9**, e1003777.
4. Bachmayr-Heyda,A., Reiner,A.T., Auer,K., Sukhbaatar,N., Aust,S., Bachleitner-Hofmann,T., Mesteri,I., Grunt,T.W., Zeillinger,R. and Pils,D. (2015) Correlation of circular RNA abundance with proliferation–exemplified with colorectal and ovarian cancer, idiopathic lung fibrosis, and normal human tissues. *Sci. Rep.*, **5**, 8057.
5. Gu,X., Li,M., Jin,Y., Liu,D. and Wei,F. (2017) Identification and integrated analysis of differentially expressed lncRNAs and circRNAs reveal the potential ceRNA networks during PDLSC osteogenic differentiation. *BMC Genet.*, **18**, 100.
6. Yu,C.Y., Li,T.C., Wu,Y.Y., Yeh,C.H., Chiang,W., Chuang,C.Y. and Kuo,H.C. (2017) The circular RNA circBIRC6 participates in the molecular circuitry controlling human pluripotency. *Nat. Commun.*, **8**, 1149.
7. Yang,D., Yang,K. and Yang,M. (2018) Circular RNA in aging and age-related diseases. *Adv. Exp. Med. Biol.*, **1086**, 17–35.
8. Zhao,Z.J. and Shen,J. (2017) Circular RNA participates in the carcinogenesis and the malignant behavior of cancer. *RNA Biol.*, **14**, 514–521.
9. Lukiw,W.J. (2013) Circular RNA (circRNA) in Alzheimer's disease (AD). *Front. Genet.*, **4**, 307.
10. Floris,G., Zhang,L., Follesa,P. and Sun,T. (2017) Regulatory role of circular RNAs and neurological disorders. *Mol. Neurobiol.*, **54**, 5156–5165.
11. Holdt,L.M., Stahringer,A., Sass,K., Pichler,G., Kulak,N.A., Wilfert,W., Kohlmaier,A., Herbst,A., Northoff,B.H., Nicolaou,A. *et al.* (2016) Circular non-coding RNA ANRIL modulates ribosomal RNA maturation and atherosclerosis in humans. *Nat. Commun.*, **7**, 12429.
12. Frontera,W.R. and Ochala,J. (2015) Skeletal muscle: a brief review of structure and function. *Calcif. Tissue Int.*, **96**, 183–195.
13. Molkentin,J.D. and Olson,E.N. (1996) Defining the regulatory networks for muscle development. *Curr. Opin. Genet. Dev.*, **6**, 445–453.
14. Das,A., Das,A., Das,D., Abdelmohsen,K. and Panda,A.C. (2019) Circular RNAs in myogenesis. *Biochim. Biophys. Acta Gene Regul. Mech.*, doi:10.1016/j.bbagrm.2019.02.011.
15. Li,Y., Chen,X., Sun,H. and Wang,H. (2018) Long non-coding RNAs in the regulation of skeletal myogenesis and muscle diseases. *Cancer Lett.*, **417**, 58–64.
16. Xu,M., Chen,X., Chen,D., Yu,B., Li,M., He,J. and Huang,Z. (2020) Regulation of skeletal myogenesis by microRNAs. *J. Cell Physiol.*, **235**, 87–104.
17. Carvalho,R.F., Cicogna,A.C., Campos,G.E., De Assis,J.M., Padovani,C.R., Okoshi,M.P. and Pai-Silva,M.D. (2003) Myosin heavy chain expression and atrophy in rat skeletal muscle during transition from cardiac hypertrophy to heart failure. *Int. J. Exp. Pathol.*, **84**, 201–206.
18. Fink,B., Egl,M., Singer,J., Fuerst,M., Bubenheim,M. and Neuen-Jacob,E. (2007) Morphologic changes in the vastus medialis muscle in patients with osteoarthritis of the knee. *Arthritis Rheum.*, **56**, 3626–3633.
19. Ottenheijm,C.A., Heunks,L.M. and Dekhuijzen,P.N. (2007) Diaphragm muscle fiber dysfunction in chronic obstructive pulmonary disease: toward a pathophysiological concept. *Am. J. Respir. Crit Care Med.*, **175**, 1233–1240.
20. Pette,D. and Staron,R.S. (2001) Transitions of muscle fiber phenotypic profiles. *Histochem. Cell Biol.*, **115**, 359–372.
21. Abdelmohsen,K., Panda,A.C., De,S., Grammatikakis,I., Kim,J., Ding,J., Noh,J.H., Kim,K.M., Mattison,J.A., de Cabo,R. and Gorospe,M. (2015) Circular RNAs in monkey muscle: age-dependent changes. *Aging*, **7**, 903–910.
22. Munk,R., Martindale,J.L., Yang,X., Yang,J.H., Grammatikakis,I., Di Germanio,C., Mitchell,S.J., de Cabo,R., Lehrmann,E., Zhang,Y. *et al.* (2019) Loss of miR-451a enhances SPARC production during myogenesis. *PLoS One*, **14**, e0214301.
23. Panda,A.C., De,S., Grammatikakis,I., Munk,R., Yang,X., Piao,Y., Dudekula,D.B., Abdelmohsen,K. and Gorospe,M. (2017) High-purity circular RNA isolation method (RPAD) reveals vast collection of intronic circRNAs. *Nucleic Acids Res.*, **45**, e116.
24. Pfaffl,M.W. (2001) A new mathematical model for relative quantification in real-time RT-PCR. *Nucleic Acids Res.*, **29**, e45.
25. Kanno,J., Aisaki,K., Igarashi,K., Nakatsu,N., Ono,A., Kodama,Y. and Nagao,T. (2006) 'Per cell' normalization method for mRNA measurement by quantitative PCR and microarrays. *BMC Genomics*, **7**, 64.
26. Kramer,M.C., Liang,D., Tatomer,D.C., Gold,B., March,Z.M., Cherry,S. and Wilusz,J.E. (2015) Combinatorial control of Drosophila circular RNA expression by intronic repeats, hnRNPs, and SR proteins. *Genes Dev.*, **29**, 2168–2182.
27. Pandey,P.R., Rout,P.K., Das,A., Gorospe,M. and Panda,A.C. (2019) RPAD (RNase R treatment, polyadenylation, and poly(A)+ RNA depletion) method to isolate highly pure circular RNA. *Methods*, **155**, 41–48.
28. Chen,Z., Viboolsittiseri,S.S., O'Connor,B.P. and Wang,J.H. (2012) Target DNA sequence directly regulates the frequency of activation-induced deaminase-dependent mutations. *J. Immunol.*, **189**, 3970–3982.
29. Chen,P., Zhao,J., Wang,Y., Wang,M., Long,H., Liang,D., Huang,L., Wen,Z., Li,W., Li,X. *et al.* (2013) H3.3 actively marks enhancers and primes gene transcription via opening higher-ordered chromatin. *Genes Dev.*, **27**, 2109–2124.
30. de Haro,H.M., Al-Ramahi,I., Jones,K.R., Holth,J.K., Timchenko,L.T. and Botas,J. (2013) Smaug/SAMD4A restores translational activity of CUGBP1 and suppresses CUG-induced myopathy. *PLoS. Genet.*, **9**, e1003445.
31. Chen,Z., Holland,W., Shelton,J.M., Ali,A., Zhan,X., Won,S., Tomisato,W., Liu,C., Li,X., Moresco,E.M. and Beutler,B. (2014) Mutation of mouse Samd4 causes leanness, myopathy, uncoupled mitochondrial respiration, and dysregulated mTORC1 signaling. *Proc. Natl. Acad. Sci. U.S.A.*, **111**, 7367–7372.
32. Niu,N., Xiang,J.F., Yang,Q., Wang,L., Wei,Z., Chen,L.L., Yang,L. and Zou,W. (2017) RNA-binding protein SAMD4 regulates skeleton development through translational inhibition of Mig6 expression. *Cell Discov.*, **3**, 16050.
33. Yanbin,Z. and Jing,Z. (2019) CircSAMD4A accelerates cell proliferation of osteosarcoma by sponging miR-1244 and regulating MDM2 mRNA expression. *Biochem. Biophys. Res. Commun.*, **516**, 102–111.
34. Ji,J., Tsika,G.L., Rindt,H., Schreiber,K.L., McCarthy,J.J., Kelm,R.J. Jr and Tsika,R. (2007) Puralpha and Purbeta collaborate with Sp3 to negatively regulate beta-myosin heavy chain gene expression during skeletal muscle inactivity. *Mol. Cell Biol.*, **27**, 1531–1543.
35. Gupta,M., Sueblinvong,V., Raman,J., Jeevanandam,V. and Gupta,M.P. (2003) Single-stranded DNA-binding proteins PURalpha and PURbeta bind to a purine-rich negative regulatory element of the alpha-myosin heavy chain gene and control transcriptional and translational regulation of the gene expression. *J. Biol. Chem.*, **278**, 44935–44948.
36. Lasham,A., Lindridge,E., Rudert,F., Onrust,R. and Watson,J. (2000) Regulation of the human fas promoter by YB-1, Puralpha and AP-1 transcription factors. *Gene*, **252**, 1–13.

37. Livi,C.M., Klus,P., Delli,P.R. and Tartaglia,G.G. (2016) catRAPID signature: identification of ribonucleoproteins and RNA-binding regions. *Bioinformatics*, **32**, 773–775.
38. Aumiller,V., Graebsch,A., Kremmer,E., Niessing,D. and Forstemann,K. (2012) Drosophila Pur-alpha binds to trinucleotide-repeat containing cellular RNAs and translocates to the early oocyte. *RNA Biol.*, **9**, 633–643.
39. Daniel,D.C. and Johnson,E.M. (2018) PURA, the gene encoding Pur-alpha, member of an ancient nucleic acid-binding protein family with mammalian neurological functions. *Gene*, **643**, 133–143.
40. Hariharan,S., Kelm,R.J. Jr and Strauch,A.R. (2014) The Puralpha/Purbeta single-strand DNA-binding proteins attenuate smooth-muscle actin gene transactivation in myofibroblasts. *J. Cell Physiol.*, **229**, 1256–1271.
41. Ohashi,S., Kobayashi,S., Omori,A., Ohara,S., Omae,A., Muramatsu,T., Li,Y. and Anzai,K. (2000) The single-stranded DNA- and RNA-binding proteins pur alpha and pur beta link BC1 RNA to microtubules through binding to the dendrite-targeting RNA motifs. *J. Neurochem.*, **75**, 1781–1790.
42. Johnson,E.M., Kinoshita,Y., Weinreb,D.B., Wortman,M.J., Simon,R., Khalili,K., Winckler,B. and Gordon,J. (2006) Role of Pur alpha in targeting mRNA to sites of translation in hippocampal neuronal dendrites. *J. Neurosci. Res.*, **83**, 929–943.
43. Gallia,G.L., Darbinian,N., Tretiakova,A., Ansari,S.A., Rappaport,J., Brady,J., Wortman,M.J., Johnson,E.M. and Khalili,K. (1999) Association of HIV-1 Tat with the cellular protein, Puralpha, is mediated by RNA. *Proc. Natl. Acad. Sci. U.S.A.*, **96**, 11572–11577.
44. Knapp,A.M., Ramsey,J.E., Wang,S.X., Godburn,K.E., Strauch,A.R. and Kelm,R.J. Jr (2006) Nucleoprotein interactions governing cell type-dependent repression of the mouse smooth muscle alpha-actin promoter by single-stranded DNA-binding proteins Pur alpha and Pur beta. *J. Biol. Chem.*, **281**, 7907–7918.
45. Johnson,E.M., Daniel,D.C. and Gordon,J. (2013) The pur protein family: genetic and structural features in development and disease. *J. Cell Physiol.*, **228**, 930–937.